Acoustic-electromagnetic slow waves in a periodical defective piezoelectric slab*

Xiao-juan Li(李小娟), Huan Ge(葛欢), Li Fan(范理)†,
Shu-yi Zhang(张淑仪), Hui Zhang(张辉), and Jin Ding(丁劲)

Laboratory of Modern Acoustics, Institute of Acoustics, Nanjing University, Nanjing 210093, *China*

(Received 22 January 2017; revised manuscript received 1 March 2017; published online 6 June 2017)

Coupled slow waves, slow acoustic waves, and electromagnetic waves are simultaneously achieved based on a piezoelectric material, in which a line defect is created within a honeycomb lattice array of cylindrical holes etched in a $LiNbO_3$ slab. Finite element simulations in frequency domain and time domain demonstrate that a highly localized slow mode is obtained in the defect. Owing to the piezoelectricity of $LiNbO_3$, acoustic and electromagnetic waves are coupled with each other and transmit along the line defect. Therefore, in addition to a slow acoustic wave, an electromagnetic wave with a group velocity even lower than conventional acoustic waves is achieved.

Keywords: piezoelectric material, phononic crystals, group velocity, slow wave

PACS: 43.38.Fx, 43.35.Cg, 43.35.Gk **DOI:** 10.1088/1674-1056/26/7/074302

1. Introduction

Slow light refers to the phenomenon in which light travels at a group velocity considerably lower than the light speed in a vacuum, which can outperform fast light in various aspects, such as optical pulse compression, nonlinear enhancement, optical switching, optical buffers or storage, among others.[1,2] The primary mechanism to realize low group velocities is to obtain small slopes in the frequency dispersion diagram on the edge of the Brillouin zone of a certain medium. Slow light devices have been created based on surface plasmon polaritons (SPPs),[3] high-quality-factor resonators,[4] and defective photonic crystals.[5,6] Compared to light, acoustic waves in solids are considered to be richer in physics because of their full vector character and the mixing of longitudinal and transverse modes.[7] Therefore, encouraged by the tremendous progress in the research of slow light, acoustic slow waves (ASWs) and acoustic confinement or trapping phenomena (ACT) were also given high consideration. ASWs were originally obtained within a corrugated metawire,[8] and the mechanism of which was an analogy with SPPs in light and electromagnetic waves. Then, an acoustic metamaterial with periodically corrugated grooves at a solid surface was presented, which realized the ACT of surface modes at different frequencies, and thus, it was defined as rainbow trapping.[9] Recently, an ultraslow-fluid-like particle employing an artificial high refractive index was presented to achieve intense Mie resonances for low-frequency airborne sound, which exhibits potential in sound insulation[10] and directional sensing.[11] In addition, a three-dimensional helical-structured acoustic metamaterial with designed inhomogeneous unit cells was used to realize a non-dispersive, high effective refractive index, in which the wavefront revolution plays a dominant role in reducing the group velocity.[12] Moreover, an anomalous Floquet topological insulator for sound was presented, which also produced a high refractive index.[13] Moreover, arrays of detuned Helmholtz resonators were used for achieving ASWs transmitting along a tube,[14,15] which can be obtained in a narrow band between the resonant frequencies of two sets of resonators with different structural parameters. Furthermore, an acoustic metamaterial was designed based on a simple and compact structure of one string of side pipes arranged along a waveguide, which simultaneously produced negative group velocities and slow waves.[16] By analogy with the defective photonic crystal, defects were induced in phononic crystal, and then, localized modes were created in the band gaps of the original phononic crystals devoid of defects.[17] According to this mechanism, one-dimensional ASWs were first obtained with a point defect induced in a one-dimensional structure.[18] In addition, ASWs at audio frequencies were obtained in a line defect fabricated in a triangular array of aluminium cylinders.[19] Despite these approaches leading to the ASWs and ACT, they have not been realized in on-chip devices, while their counterparts for slow light have been reported.[4,20]

Piezoelectric materials are widely applied in the fabrication of on-chip acoustic devices based on the technology of Miro-Electromechanical Systems (MEMS),[21–23] as filters, resonators, sensors, and the like. Although piezoelectricity-based phononic crystals with or without defects were pre-

*Project supported by the National Basic Research Program of China (Grant No. 2012CB921504), the National Natural Science Foundation of China (Grant Nos. 11374154, 10904067, and 11174142), the Natural Science Foundation of Jiangsu Province of China (Grant No. BK20151375), and the Special Fund for Research in Quality Inspection of Public Welfare Industry, China (Grant No. 201510068).

†Corresponding author. E-mail: fanli@nju.edu.cn

© 2017 Chinese Physical Society and IOP Publishing Ltd

sented for the realization of acoustic forbidden bands[24–27] and guiding-wave modes,[28–30] the ASWs and ACT have not been created based on piezoelectric materials.

In this study, we present a defective periodical structure based on an $LiNbO_3$ slab, in which the ACT and ASWs can be achieved, resulting in a signal expanding in the time domain and a group velocity more than 17 times lower than the velocity of the conventional flexural plate mode transmitting in an $LiNbO_3$ plate. Furthermore, owing to the coupling of acoustic fields and electromagnetic fields in the $LiNbO_3$ piezoelectric material, slowdown and trapping for electromagnetic waves can also be achieved. Therefore, slow acoustic waves and electromagnetic waves are simultaneously realized in the structure. In particular, by virtue of the extremely large difference between the velocities of elastic waves and electromagnetic waves, the slowdown of the electromagnetic wave in this structure can be considerably larger than those in pure electromagnetic devices, which produces an electromagnetic wave with the group velocity even lower than that of the conventional acoustic waves in solids. Therefore, simultaneous manipulations of acoustic fields and electromagnetic fields can be realized based on the presented piezoelectricity-based on-chip structure.

2. Model and theory

To design the on-chip device to create the coupled slow waves, first, a periodical structure is established on the basis of an $LiNbO_3$ slab, in which a honeycomb lattice array of cylindrical holes is etched. The thickness, width, and length of the slab are $d = 12$ μm, $b = 197$ μm, and $l = 700$ μm, respectively. The material parameters of $LiNbO_3$ are listed in Table 1.[31]

Figure 1(a) shows one unit cell in the periodical structure, in which the x-axis is along the longer diagonal of the smallest hexagon built up by the etched holes and the z-axis is perpendicular to the surface of the slab. The geometric parameters of the structure are the lattice constant of $a = 15$ μm, the radius of the cylindrical hole, $r = 6.4$ μm, which is the slab from the top to the bottom. The filling ratio of the structure is defined as $\mathrm{FR} = 4\sqrt{3}\pi r^2/9a^2$, which is 44% according to the designed parameters. In addition, two identical thin aluminium sheets are attached to the top and bottom of the slab as electrodes to excite electric signals. Figure 1(b) shows the irreducible Brillouin zone of the honeycomb lattices in the structure. The finite element simulations with COMSOL Multiphysics are used to calculate the dispersion and frequency bands of the periodical structure. By scanning the wave vector along the edge of the irreducible Brillouin zone and solving the eigenvalue problems for each wave vector, the eigenfrequencies of the periodic structure can be obtained as well as the dispersion curve. Figure 1(c) shows the simulated band structure of the piezoelectric phononic crystal along the edge of the irreducible Brillouin zone, which exhibits a wide complete band gap from 89 MHz to 111 MHz for the coupled acoustic-electromagnetic wave. The intended design of the structural parameters ensures that the band gap is located in the working frequency ranges of the majority of ultrasonic devices, which makes it compatible to conventional MEMS devices.

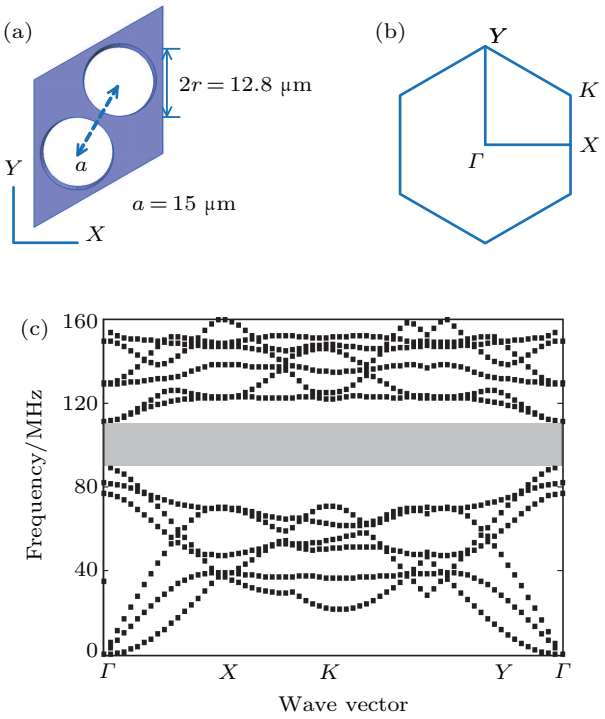


Fig. 1. (color online) (a) A unit cell of the phononic crystal based on an $LiNbO_3$ slab with periodically etched cylindrical holes; r and a are the radius of the holes and the lattice constant, respectively. (b) The irreducible Brillouin zone for the hexagonal lattices. (c) The band structure of the phononic crystal slab with hexagonal lattices calculated by COMSOL with the parameters of $d = 12$ μm, $a = 15$ μm, and $r = 6.4$ μm. The shaded part indicates the complete phononic band gap obtained in the structure.

Table 1. Parameters of $LiNbO_3$ material adopted in the simulations.

Property		Value		Value
Elastic constant	c_{11}	20.3×10^{10} N/m^2	c_{14}	0.9×10^{10} N/m^2
	c_{12}	5.3×10^{10} N/m^2	c_{33}	24.5×10^{10} N/m^2
	c_{13}	7.5×10^{10} N/m^2	c_{44}	6.0×10^{10} N/m^2
Piezoelectric constant	e_{15}	3.7 C/m^2	e_{22}	2.5 C/m^2
	e_{31}	0.2 C/m^2	e_{33}	1.9 C/m^2
Dielectric constant	$\varepsilon_{11}/\varepsilon_0$	84	$\varepsilon_{33}/\varepsilon_0$	30
Density	ρ	4700 kg/m^3		

To achieve the effects of slow wave and trapping, a line defect is induced into the periodical structure by filling one row of holes in the etched $LiNbO_3$ slab, as shown in Fig. 2(a). The line defect is parallel to the x axis, which is the propagation direction of the coupled waves in the slab. The x and z axes are consistent with the x and z crystallographic orientations of $LiNbO_3$. Because of the piezoelectricity of $LiNbO_3$, the acoustic and electromagnetic waves are coupled in the slab,

which can be expressed by the wave equations for acoustic and electromagnetic waves, respectively[31]

$$\nabla_{iK} c_{KL} \nabla_{Lj} u_j - \rho \frac{\partial^2 u_i}{\partial t^2} = -\nabla_{iK} e_{Kj} \nabla_j \frac{\partial \phi}{\partial t}, \quad (1)$$

$$\nabla_i \varepsilon_{ij} \nabla_j \frac{\partial^2 \phi}{\partial t^2} = \nabla_i e_{iL} \left(\nabla_{Lj} \frac{\partial u_j}{\partial t} \right), \quad (2)$$

where ρ is the density, and c_{KL}, e_{Kj}, and ε_{ij} (i, j = 1–3 and K, L = 1–6) are the elastic, piezoelectric, and dielectric constants of $LiNbO_3$ material, respectively. u_j and ϕ are the particle displacement and electric potential in the slab, which are related to the acoustic and electromagnetic fields, respectively. Then, both fields in the slab can be expressed in the same form of $u_j = A_j \exp[j(k_x x + k_z z - \omega t)]$ or $\phi = A_4 \exp[j(k_x x + k_z x_z - \omega t)]$, where k_x and k_z are the wave numbers in the x and z directions, respectively; ω and t are the angular frequency and time, respectively; and A_j and A_4 are the amplitudes of the particle displacement and electric potential, respectively. It can be determined that the acoustic and electromagnetic fields are coupled with each other in the slab, and they can be excited by electric or acoustic sources. Therefore, for the realization of an on-chip device, two aluminium strips are set up on one terminal of the $LiNbO_3$ slab, working as a pair of (top and bottom) electrodes. Thus, the coupled acoustic and electromagnetic fields can be simultaneously excited by the electric signal exerted on the electrodes, which is a similar excitation method to those used in conventional on-chip MEMS devices. Owing to the line defect, the periodicity along the y direction is broken in the structure, and then the defective structure is considered to be composed of 16 supercells periodically arranged along the x direction, as shown in Fig. 2. In the calculation of the band structure, periodical boundary conditions are applied on both sides of the supercells shown in Fig. 2(b).

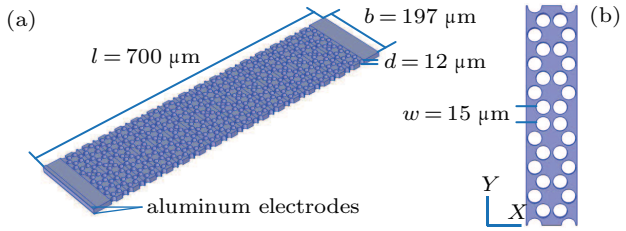


Fig. 2. (color online) (a) Piezoelectric $LiNbO_3$ slab with a line defect in the middle: three periods of honeycomb lattices are set up on both sides of the line defect and 16 periods of the supercells are arranged along the direction of the line defect (x direction). A pair of aluminium stripes (top and bottom electrodes) is set up on one terminal of the slab for inputting excitation signals. (b) A supercell of the structure, with w being the width of the defect.

The simulated band structure of the wave transmission along the x direction of the defective structure is shown in Fig. 3(a). Compared to the band structure shown in Fig. 1(c), it is observed that several transmitting modes can be excited in the forbidden band of the original defect-free phononic crystal, which are the modes induced by the line defect. In particular, with an optimized width of the line defect $w = 15$ μm, a unique mode exhibiting an isolated flat band, which is marked out by the circles in Fig. 3(a), is achieved. This mode lies in a narrow frequency band between 102.5 MHz and 103.8 MHz, and thus, it exhibits an extremely low group velocity v_g according to the definition of $v_g = \partial\omega/\partial k_x$, which is a slow wave. In addition, as shown in Fig. 3(a), based on the designed parameters, this mode is completely isolated from other guided modes. Therefore, the mode can be solely excited easily in the $LiNbO_3$ slab by restricting the exciting frequency in the narrow band, which ensures the simplification of the practical application.

3. Discussion and result

Figures 3(b) and 3(c) show the profiles of the acoustic and electromagnetic fields, respectively, in a supercell with the exciting eigenfrequency of 103.5 MHz and at the edge of the irreducible Brillouin zone. It is found that a highly localized mode is obtained in the line defect, corresponding to the flat pass band indicated in Fig. 3(a). Furthermore, a frequency-domain simulation is taken based on the defective structure composed of 16 supercells. Figures 3(d) and 3(e) exhibit the distributions of the acoustic and electromagnetic fields in the structure excited by a sinusoidal electric signal with a frequency of 103.5 MHz. It is demonstrated that both acoustic and electromagnetic fields are highly constrained within the line defect, which are localized modes transmitting along the defect.

To demonstrate the performance of the localized modes, time-domain simulations are taken to study the transmissions of the waves in the line defect. A sinusoidal wave enveloped by a Gaussian pulse with the 3 dB bandwidth of 0.05 μs is used as the excitation, as indicated in Fig. 4(a). The central frequency of the pulse is chosen to be 103.5 MHz, which is within the frequency range of the isolated local mode indicated by the frequency-domain simulations. The Gaussian envelope contains six cycles of the sinusoidal signal. Figure 4(b) shows the normalized time domain signals of the acoustic field extracted from two points (1 and 2). Both points are on the surface of the slab and in the centre of the line defect, and the distances between them and the aluminium electrode are $6a$ and $24a$, respectively. It is observed that the envelope shapes of the extracted signals are similar to that of the exciting signal, which exhibits the propagating process of the acoustic field in the line defect. The 3 dB bandwidths of the acoustic signals extracted from both points are approximately 1 μs, which demonstrate that the source pulse is expanded by 20 times in the time domain, compared to the excitation signal width of 0.05 μs. Moreover, figure 4(c) shows the signals for the electromagnetic field extracted from points 1 and 2, which exhibits similar time-domain distributions to those

of the acoustic fields. Therefore, it is demonstrated that remarkable trapping effects induced by multiple scattering in this periodic structure for both acoustic and electromagnetic fields are achieved in the structure. The group velocities of the acoustic and electromagnetic waves can be achieved from the time difference corresponding to the peaks of the signals obtained at points 1 and 2 indicated in Fig. 4. To more accurately determine the group velocity, a series of extracting points is set up along the line defect, in which the distance between the neighboring points remains $9a$.

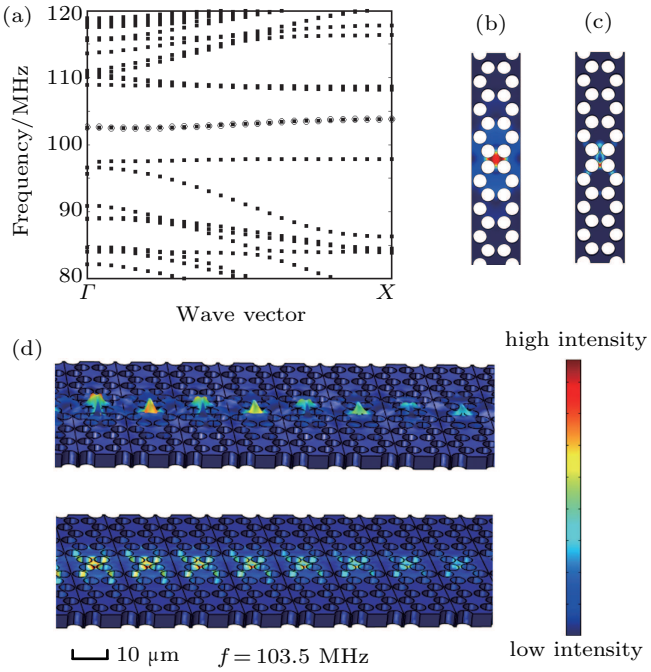


Fig. 3. (color online) (a) Dispersion of the structure with the width of the line defect $w = 15$ μm, in which the isolated mode with a flat pass band is marked by circles. The profile of the localized modes with the frequency of 103.5 MHz for acoustic field (b) and electromagnetic field (c) in one supercell. (d) Acoustic field (the strain is magnified for clarity) and (e) electromagnetic field at the frequency of 103.5 MHz transmitting along the line defect obtained by the frequency-domain simulations.

Figure 5 shows the transmitting time versus the distances from the electrode for every extracting point. It is indicated that the transmitting time is linearly dependent on the distances, which demonstrates that the pulse signal travels with a constant group velocity. Then, the group velocity can be obtained from the reciprocal of the slope of the fitted line for the five extracting points, which is calculated to be $v_g = 181$ m/s and is in accordance with the group velocity deduced from the dispersion curve shown in Fig. 3. According to the theory concerning acoustic transmissions in piezoelectric materials, it can be obtained that the velocities of ultrasonic waves in the $LiNbO_3$ slab are 7400 m/s for the longitudinal wave, 3592 m/s for the surface acoustic wave, and 3046 m/s for the flexural plate mode with a frequency of 103 MHz. Then, it can be determined that the group velocity achieved in the presented structure is less than $1/17$ of the velocities of the conventional acoustic waves in $LiNbO_3$. According to the refractive index $n = 2.32$ of electromagnetic waves in $LiNbO_3$, the velocity of the conventional electromagnetic wave transmitting in a $LiNbO_3$ slab can be calculated to be 1.29×10^8 m/s. Therefore, the guided electromagnetic wave in the line defect with a group velocity of $v_g = 181$ m/s is slowed down by more than

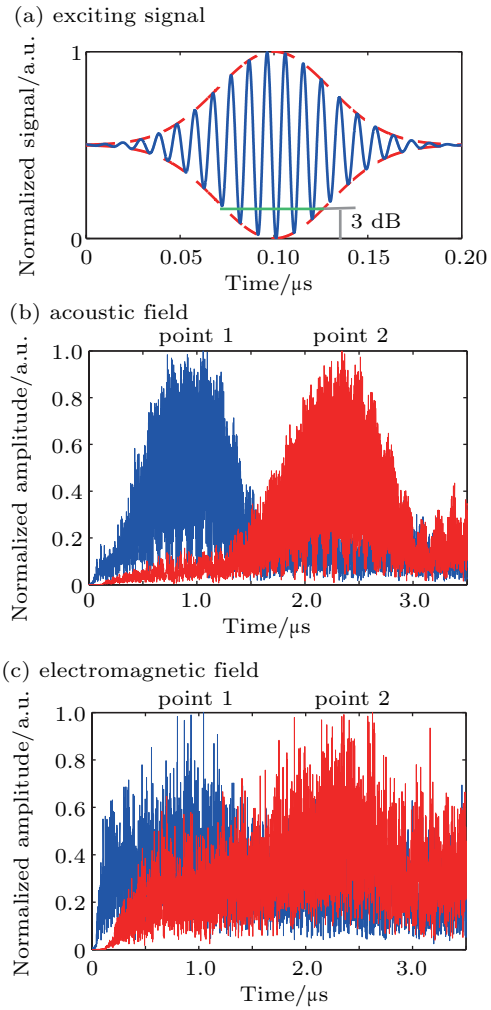


Fig. 4. (color online) (a) Waveform of the pulse signal exerted on the top electrode at the input terminal of the slab. Normalized amplitudes of time-domain acoustic field (b) and electromagnetic field (c) extracted at points 1 and 2 within the line defect, the distances between the aluminium electrodes and points 1 and 2 are, $6a$ and $24a$, respectively.

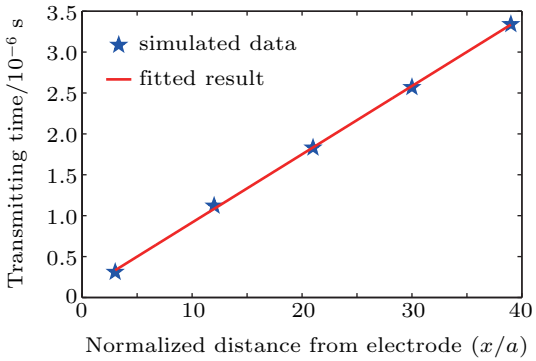


Fig. 5. (color online) Transmitting time versus the distances from the electrodes for five extracting points. The solid line indicates the linearly fitted result, from which the group velocity can be calculated to be $v_g = 181$ m/s.

7.10×10^5 times by virtue of the coupling with the slow acoustic wave, which demonstrates a considerably higher rate of slowdown than those obtained in slow wave devices based on pure electromagnetic fields. Therefore, coupled slow waves, namely, slow acoustic and electromagnetic waves, can be simultaneously achieved in the structure.

4. Conclusions

In conclusion, the phenomena of energy trapping and slow waves are achieved in an on-chip $LiNbO_3$ slab with a structure composed of a honeycomb lattice array of cylindrical holes with a line defect. Owing to the piezoelectricity of the $LiNbO_3$ slab, the energy trapping and slowdown effects are simultaneously realized in both acoustic and electromagnetic waves, which is defined to be double slow waves. It is observed that the width of the exciting Gaussian signal is widened by 20 times, indicating an effect of the ACT. Meanwhile, the group velocity of acoustic waves in the structure is also slowed down by 17 times, which is an ASW. Moreover, by virtue of the giant difference between the transmitting velocities of acoustic and electromagnetic fields, the transmission of the electromagnetic wave coupled with the acoustic wave in the structure can be remarkably slowed down by 7.10×10^5 times. Consequently, an electromagnetic wave transmitting even slower than a conventional surface acoustic wave in a solid plate is achieved. Therefore, acoustic and electromagnetic waves can be simultaneously manipulated based on this on-chip piezoelectric slab, which demonstrates great potential for MEMS devices such as delay lines and sensors, as well as electromagnetic devices such as data processors and spectrometers.

References

[1] Parra E and Lowell J R 2007 *Opt. Photon. News* **18** 41
[2] Krauss T F 2008 *Nat. Photon.* **2** 448
[3] Gan Q Q, Gao Y K, Wagner K, Vezenov D, Ding Y J and Bartoli F J 2011 *PNAS* **108** 5169
[4] Xu Q F, Dong P and Lipson M 2007 *Nat. Phys.* **3** 406
[5] Noda S, Chutinan A and Imada M 2000 *Nature* **407** 608
[6] Vlasov Y A, O'boyle M, Hamann H F and Mcnab S J 2005 *Nature* **438** 65
[7] Kafesaki M, Sigalas M M and García N 2000 *Phys. Rev. Lett.* **85** 4044
[8] Christensen J, Huidobro P A, Martín-moreno L and García-vidal F J 2008 *Appl. Phys. Lett.* **93** 083502
[9] Zhu J, Chen Y Y, Zhu X F, Garcia-vidal F J, Yin X B, Zhang W L and Zhang X 2013 *Sci. Rep.* **3** 1728
[10] Cheng Y, Zhou C, Yuan B G, Wu D J, Wei Q and Liu X J 2015 *Nat. Mater.* **14** 1013
[11] Zhu X F, Liang B, Kan W W, Peng Y G and Cheng J C 2016 *Phys. Rev. Appl.* **5** 054015
[12] Zhu X F, Li K, Zhang P, Zhu J, Zhang J T, Tian C and Liu S C 2016 *Nat. Commun.* **7** 11731
[13] Peng Y G, Qin C Z, Zhao D G, Shen Y X, Xu X Y, Bao M, Jia H and Zhu X F 2016 *Nat. Commun.* **7** 13368
[14] Santillan A and Bozhevolnyi S I 2011 *Phys. Rev. B* **84** 064304
[15] Santillan A and Bozhevolnyi S I 2014 *Phys. Rev. B* **89** 184301
[16] Li X J, Xue C, Fan L, Zhang S Y, Chen Z, Ding J and Zhang H 2016 *Appl. Phys. Lett.* **108** 231904
[17] Hsiao F L, Khelif A, Moubchir H, Choujaa A, Chen C C and Laude V 2007 *Phys. Rev. E* **76** 056601
[18] Robertson W M, Baker C and Bennett C B 2004 *Am. J. Phys.* **72** 255
[19] Cicek A, Kaya O A, Yilmaz M and Ulug B 2012 *J. Appl. Phys.* **111** 013522
[20] Yanik M F and Fan S H 2007 *Nat. Phys.* **3** 372
[21] Mohammadi S, Eftekhar A A, Khelif A, Hunt W D and Adibi A 2008 *Appl. Phys. Lett.* **92** 221905
[22] Vasseur J O, Hladky-hennion A C, Djafari-rouhani B, Duval F, Dubus B and Pennec Y 2007 *J. Appl. Phys.* **101** 114904
[23] Mohammadi S, Eftekhar A A, Hunt W D and Adibi A 2009 *Appl. Phys. Lett.* **94** 051906
[24] Wilm M, Khelif A, Laude V and Ballandras S 2007 *J. Acoust. Soc. Am.* **122** 786
[25] Vatanabe S L, Paulino G H and Silva E C N 2014 *J. Acoust. Soc. Am.* **136** 494
[26] Degraeve S, Granger C, Dubus B, Vasseur J O, Thi M P and Hladky A C 2015 *Smart Mater. Struct.* **24** 085013
[27] Achaoui Y, Khelif A, Benchabane S and Laude V 2010 *J. Phys. D: Appl. Phys.* **43** 185401
[28] Yamauchi N, Shirai T, Yoshihara T, Hayasaki Y, Ueda T, Matsushima T, Wasa K, Kanno I and Kotera H 2009 *Appl. Phys. Lett.* **94** 172903
[29] Lin C M, Lien W C, Felmetsger V V, Hopcroft M A, Senesky D G and Pisano A P 2010 *Appl. Phys. Lett.* **97** 141907
[30] Wasa K, Matsushima T, Adachi H, Kanno I and Kotera H 2012 *J. Microelectromech. S.* **21** 451
[31] Auld B A 1973 *Acoustic Fields and Waves in Solid* (New York: John Wiley & Sons)